The Journal of Chemical Physics

An efficient water force field calibrated against intermolecular THz and Raman spectra

Cite as: J. Chem. Phys. **148**, 244504 (2018); https://doi.org/10.1063/1.5037062
Submitted: 20 April 2018 • Accepted: 05 June 2018 • Published Online: 25 June 2018

David Sidler, Markus Meuwly and Peter Hamm

AIP Publishing

An efficient water force field calibrated against intermolecular THz and Raman spectra

David Sidler,[1] Markus Meuwly,[2] and Peter Hamm[1]
[1]*Department of Chemistry, University of Zurich, Zurich, Switzerland*
[2]*Department of Chemistry, University of Basel, Basel, Switzerland*

(Received 20 April 2018; accepted 5 June 2018; published online 25 June 2018)

A polarizable water model is presented which has been calibrated against experimental THz and Raman spectra of bulk water. These low-frequency spectra directly probe the dynamics, and thereby intermolecular interactions, on time scales relevant to molecular motions. The model is based on the TL4P force field developed recently by Tavan and co-workers [J. Phys. Chem. B **117**, 9486 (2013)], which has been designed to be transferable between different environments; in particular, to correctly describe the electrostatic properties of both the isolated water molecule in the gas-phase and the liquid water at ambient conditions. Following this design philosophy, TL4P was amended with charge transfer across hydrogen-bonded dimers as well as an anisotropic polarizability in order to correctly reproduce the THz and Raman spectra. The thermodynamic and structural properties of the new model are of equal quality as those of TL4P, and at the same time, an almost quantitative agreement with the spectroscopic data could be achieved. Since TL4P is a rigid model with a single polarizable site, it is computationally very efficient, while the numerical overhead for the addition of charge transfer and the anisotropic polarizability is minor. Overall, the model is expected to be well suited for, e.g., large scale simulations of 2D-Raman-THz spectra or biomolecular simulations. *Published by AIP Publishing.* https://doi.org/10.1063/1.5037062

I. INTRODUCTION

Although being a fairly simple molecule, water exhibits very complex behavior in the condensed phase with many anomalies in its thermodynamic properties whose origin still is a matter of debate.[1,2] These anomalies play a crucial role for understanding solvation effects on various processes. Vibrational spectroscopy can be applied to gain information about its structure and dynamics. From mid-IR spectra measuring the intramolecular degrees of freedom of the water molecule, one can draw conclusions about the surroundings of individual water molecules from the lineshape function of the absorption peaks. 2D IR spectroscopy can be used to distinguish contributions of homogeneous and inhomogeneous broadening of the environment, and as such insights about the dynamics of the environment can be gained.[3–10]

By contrast, spectroscopy in the THz regime directly probes the inter-molecular dynamics (MD) of the hydrogen bonding network of water and can potentially resolve the structural heterogeneity within bulk water to a certain extent. The modes in the THz range are very delocalized,[11] and it is difficult to distinguish between an oscillator and its environment. Furthermore, the water molecules move in a very anharmonic potential, and the lifetime of hydrogen bonds was reported to be in the range of ≈1 ps.[12] This inhomogeneous and very dynamic environment causes strong broadening of all spectral features. The THz absorption spectrum [Fig. 1(b), black line] has three to a certain extent distinct bands,[13] which are interpreted by the modes illustrated in Fig. 1(a). The maximum intensity band at 600 cm^{-1} arises from librational modes (hindered rotation), the weaker band at 200 cm^{-1} belongs to hydrogen bond vibrations, and a faint shoulder at 50 cm^{-1} originates from hydrogen bond bending modes. The Raman spectra show the same three bands but with very different relative intensities [Fig. 1(c), black line].[14] Higher order THz spectroscopy has the potential to better resolve the spectral features and thereby refine these assignments.[15] Currently, 2D-Raman-THz is the only 2D method in this spectral range that has successfully been applied to water[16] and aqueous salt solutions,[17] but the interpretation of these nonlinear responses remains a challenge.

Computer simulations can contribute to a microscopic understanding of the THz and Raman responses. Due to the large anharmonicity of the intermolecular degrees of freedom of liquid water, a description based on harmonic normal modes is problematic.[18,19] However, the low frequency of the motions around k_BT makes classical molecular dynamics (MD) a good tool to model these intermolecular vibrations, thereby capturing the full anharmonicity of the intermolecular potential. MD simulations directly follow the time-evolution of the system, and the calculation of various space and time correlation functions is straightforward in principle.[20] It is desirable to use MD simulations to derive relationships between spectral features and molecular structure and motions on a microscopic scale.[21]

The simulation of response functions in the THz range requires a water model with the following properties. First, as is true for any water force field, it should accurately represent the intermolecular energies, from which realistic forces, structures, and dynamics are generated. Furthermore,

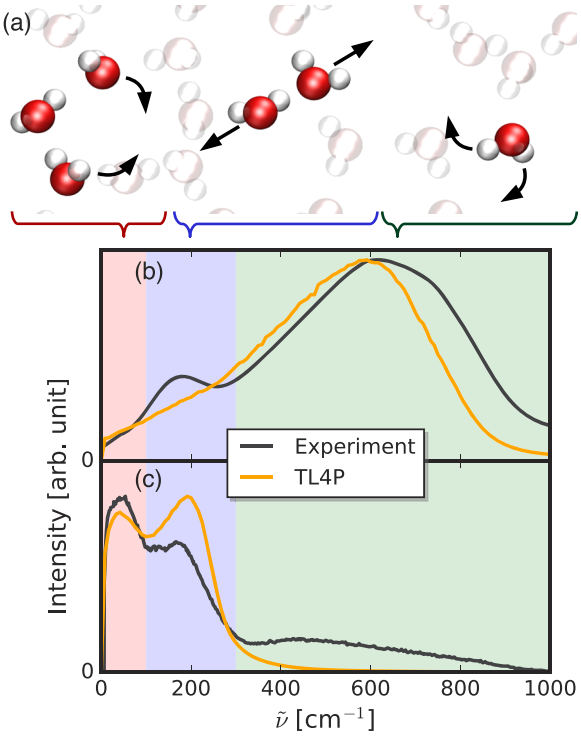

FIG. 1. (a) Illustration of the vibrational modes associated for the three bands visible in the THz range (the vibrations might be more delocalized in reality). (b) Experimental THz absorption spectrum of water (multiplied with the experimental refractive index) at 25 °C (black),[13] compared to that calculated from the TL4P model (orange).[20] (c) The same for the anisotropic Raman spectrum measured by optical Kerr effect spectroscopy.[14]

in order to simulate a Raman spectrum, which is related to the autocorrelation function of the polarizability, the water model needs to be polarizable. A multitude of polarizable water force fields have been developed, treating polarizability in many different ways, i.e., Drude oscillator models,[22–27] first principle water models,[28–30] models including three-body interactions explicitly,[31,32] fluctuating charge models,[33,34] and models with an inducible dipole moment[35–44] or higher electrostatic moments.[38,45,46] Beyond that—and that is no longer standard for most water models—the electrostatic properties need to be fine-tuned to reproduce accurate transition dipoles as well as transition polarizabilities so that the relative intensities in the THz and Raman spectra agree with experiment. Moreover, the simulation of higher order response functions requires very extensive sampling of phase space, for which simulation times of a few 100 μs are needed; computational efficiency of the model thus is very important. The purpose of this work is to develop a water model that fulfills all these criteria.

In order to avoid the "polarization catastrophe," most polarizable water force fields use a polarizability that is smaller than the experimental value of 1.47 Å^3; for example, SWM4-NDP uses 0.98 Å^3.[24] However, such a model can only poorly describe the interaction with the homogeneous electric field from a laser pulse needed for the Raman response. Applying a damping to the dipole-dipole interaction at short distances with a Thole-type interaction[47] can circumvent this problem. A Gaussian inducible dipole has the same effect,[48,49] which is the basis of a series of water models recently introduced by Tavan and co-workers.[44,50] As a cornerstone in the design of these models, the dipole moment and polarizability of an isolated water molecule were set to the experimental gas phase value. This design philosophy ensures that the models are transferable to different environments and, as a side aspect, also correctly account for a Raman interaction with an external laser field. The models are furthermore rigid and thus computationally efficient. We, in turn, have argued that 2D-Raman-THz spectroscopy is particularly sensitive to the correct description of the polarizability of a force field and have shown that amongst different off-the-shelf water models tested, the TL4P model[50] gave the best agreement with the experimental 2D-Raman-THz response.[20] We therefore think that TL4P is a good starting point for a "spectroscopic force field" that focuses on the inter-molecular degrees of freedom in the THz range.

Here, we aim at further improving TL4P as a spectroscopic force field. Figure 1 (orange *versus* black lines) shows that TL4P does not even fully reproduce the (1D) THz absorption and Raman spectra, which certainly should be considered a minimum requirement for modeling 2D-Raman-THz spectroscopy. Two major differences catch the eye: First, the 600 cm^{-1} band in the Raman spectrum is completely missing in the TL4P simulations since the polarizability in TL4P is assumed to be isotropic. The 600 cm^{-1} band is a librational mode, i.e., a hindered rotation of individual water molecules. In order that such a rotation changes the polarizability of a water molecule in the laboratory frame, and thereby renders that degree of freedom visible in the Raman spectrum, the polarizability needs to be anisotropic. Second, the simulated THz absorption spectrum severely underestimates the intensity of the 200 cm^{-1} band. It is well known that a point charge model (such as TIP4P/2005[51]) misses the hydrogen bond vibration completely since two fixed dipoles vibrating against each other will not change the overall dipole.[11] That is, while the corresponding mode exists in MD simulations of a point charge model, it does not have any transition dipole. Polarizability introduces a transition dipole of that vibration; since the overall dipole is modulated with the intermolecular distance, however, TL4P underestimates the intensity of this band severely.

The purpose of this paper is to amend the electrostatics of the TL4P model,[50] in such a way that both bands obtain a realistic transition polarizability and transition dipole, respectively. For the Raman band at 600 cm^{-1}, we need to allow for an anisotropic polarizability. Experimentally, the polarizability of an isolated water molecule is nearly isotropic. While the polarizability is commonly assumed to be isotropic in water force fields, its anisotropy is a crucial aspect in the description of the Raman spectrum.

As for the intensity of the THz band at 200 cm^{-1}, we add charge transfer to the TL4P model. It is well established that hydrogen bonding causes a small amount of charge to flow from the hydrogen bond acceptor to the hydrogen bond donor.[27,52–58] It has been demonstrated by Torii that a very simple treatment of this effect, where the transferred charge is defined as a function of the hydrogen bond length, can capture the intensity of the hydrogen bond vibration band.[58] In these simulations, however, separate sets of charges were

used for the force field and for the calculation of the THz spectrum. A similar approach was taken by Tanimura and co-workers, who concentrated on the effect of charge transfer on the Raman spectra.[43] However, it is desirable to have one and the same force field for the MD simulation as well as the calculation of the spectroscopy.[21] To that end, Rick and co-workers have developed a way to integrate charge flow into a force field in a self-consistent manner[59] and applied it to a Drude model.[27]

In this paper, a total of three new force fields are parametrized, verified with respect to their thermodynamic properties, and THz absorption and anisotropic Raman spectra are calculated: the TL4P^{i}-CT model, which adds charge flow across a hydrogen bond to the TL4P model in a self-consistent manner but still assumes an isotropic polarizability, TL4P^{a1}-CT, for which in addition the polarizability has been replaced by the experimental anisotropic polarizability tensor, and TL4P^{a2}-CT, which reduces the anisotropy of the polarizability in such a way that the intensity of the 600 cm^{-1} Raman band matches experiment. We will see that TL4P^{a2}-CT reveals almost perfect THz absorption and Raman spectra, setting the stage for an in-depth investigation of the various features observed in 2D-Raman-THz spectroscopy.[16]

II. SIMULATION DETAILS

All MD simulations were performed with a home-written MD code. If not stated otherwise, the systems simulated were cubic boxes containing 256 water molecules under periodic boundary conditions. Long-range electrostatic interactions were treated by Ewald summation,[49] with the dielectric constant of the surrounding continuum set to the experimental value of $\epsilon_{RF} = 78$. The van der Waals potentials were switched to zero between 8.55 Å and 9.5 Å, and a long-range correction term for energy and pressure of the van der Waals potential was applied.[60] The inducible dipole moments were calculated according to

$$\boldsymbol{\mu}_i = \boldsymbol{\alpha}_i \left(\boldsymbol{E}_{ext} + \sum_{j \neq i} \left(\boldsymbol{E}_j + \boldsymbol{T}_{ij} \boldsymbol{\mu}_j \right) \right), \tag{1}$$

where $\boldsymbol{\mu}_i$ is the induced dipole of water i, $\boldsymbol{\alpha}_i$ is its polarizability in the laboratory frame, $\boldsymbol{E}_j$ is the electrical field the point charges of water j produce at the position of water i, $\boldsymbol{T}_{ij}$ is the dipole-dipole interaction tensor, and $\boldsymbol{E}_{ext}$ is an external field needed to calculate the Raman response (it was switched off during the force calculation in the MD simulation). Equation (1) was solved iteratively for the $\boldsymbol{\mu}_i$ until the changes are less than 10^{-6} e Å, which took in average 6 iterations (the computational cost of that iteration is about 3 times that for the point charges and van der Waals interactions). The equation of motion was integrated using a velocity Verlet algorithm[61] with a time step of 1 fs. The geometry of the water molecules was constrained using the M-SHAKE algorithm.[62] All simulations were carried out in the *NVT* ensemble at density ρ = 0.9965 g/cm^3 and temperature 300 K, where the temperature was controlled with a velocity rescaling thermostat with a coupling time of 1 ps.[63] The instantaneous pressure was calculated using the virial expression.[64] Varying simulation lengths ranging from 500 ps to 50 ns have been used for the different tasks (which are specified below), depending on the desired accuracy of a particular property and how quickly it converges. Error bars have been determined by block averaging.

All density functional theory (DFT) calculations were performed with the Gaussian plane wave formalism implemented in the CP2K program.[65,66] As in Tavan's work,[44,50] the exchange- and correlation functional of Perdew, Burke, and Ernzerhof (PBE) was used.[67] The electron density was expanded in augmented quadruple zeta basis sets with three sets of polarization functions for both H and O atoms.[68] Only the electrons of the outermost shell were treated explicitly, while the core electrons were treated by Goedecker-Teter-Hutter pseudopotentials.[69,70] The considered water clusters were centered into a box with size 15 Å under non-periodic boundary conditions with a plane wave basis cutoff of 150 Ry.

III. PARAMETRIZATION

A. TL4P model

As all water models developed here start from TL4P,[50] we first introduce this model. TL4P is a rigid water model with the atoms fixed to the experimental liquid phase geometry (r_{OH} = 0.968 Å, bond angle θ = 105.3°). The electrostatic interactions are arising from three point charges, two of which are located on the hydrogen atoms and one on a massless point M that is displaced from the oxygen atom (see Fig. 2). Furthermore, a Gaussian polarizable site is placed on the oxygen atom with an isotropic polarizability that matches the experimental value α_{iso} = 1.47 Å.[71] The charges q_M and q_H and the distance l_{OM} of site M from the oxygen atom are constrained such that the molecule has no net charge and that the dipole moment of an isolated water molecule agrees with the experimental gas phase value μ = 1.855 D. The two remaining free parameters determining the electrostatics, l_{OM} and the width of the Gaussian σ, were fit such that the electrostatic moments of a water molecule in a realistic liquid phase environment agree best with a DFT water molecule placed in the same environment.[50]

The Pauli repulsion and van der Waals interactions are modeled with a Buckingham potential acting between oxygen atoms,

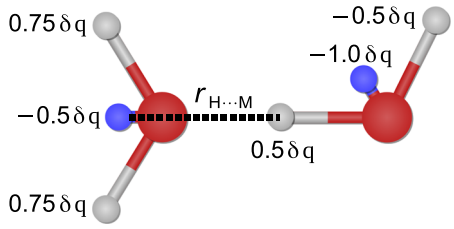

FIG. 2. Redistribution of the charge $\delta q(r_{H\cdots M})$ [which is calculated from Eq. (3)] among the atoms of the two waters of a hydrogen bonded dimer. The red spheres are oxygen atoms, the white spheres are hydrogen atoms, and the blue spheres represent the massless dummy particles M. In addition to these charge transfers, the hydrogen atom and the dummy particle carry the point charges q_H and q_M, respectively, reported in Table I.

$$V_{\mathrm{VdW}}(r) = A_1 \exp(-A_2 r) - B/r^6. \quad (2)$$

The Buckingham parameters were empirically fit to match the following experimental quantities, all at density $\rho = 0.9965$ g/cm^3 and temperature 300 K: the position of the first peak in the O–O radial distribution function (RDF) ($r_{\max} = 2.76$ Å), the pressure ($p = 1$ bar), and the average potential energy per water molecule ($\langle E_{\mathrm{pot}} \rangle = -9.92$ kcal/mol).[72]

B. Charge transfer

The amount of overall charge δq transferred across a hydrogen bond is defined as a function of the hydrogen bond distance $r_{\mathrm{H}\cdots\mathrm{M}}$, for which we chose a single sided parabola,

$$\delta q(r_{\mathrm{H}\cdots\mathrm{M}}) = \begin{cases} \frac{1}{2} q_{\mathrm{CT}} (r_{\mathrm{H}\cdots\mathrm{M}} - r_{\mathrm{CT}})^2 & \text{if } r_{\mathrm{H}\cdots\mathrm{M}} < r_{\mathrm{CT}} \\ 0, & \text{otherwise} \end{cases}. \quad (3)$$

Torii has shown that this functional form gives an electron population derivative that agrees well with quantum chemistry calculations.[58] For each pair of water molecules, four intermolecular H$\cdots$M distances exist in principle along the lines of Eq. (3), yet, typically only one contributes in a pair of hydrogen-bonded waters, since the cutoff r_{CT} is very small (*vide infra*). Based on quantum-chemistry calculations,[27,54] it has been suggested to redistribute that charge transfer $\delta q(r_{\mathrm{H}\cdots\mathrm{M}})$ among the atoms of the two water molecules, as illustrated in Fig. 2.

Expressions for energy and force contributions have been derived by Rick and co-workers.[59] Their numerical implementation is a bit tedious but straightforward. We have verified the correctness of our implementation by testing the energy stability in an *NVE* run with very tight convergence criteria. For both TL4P and TL4P$^{\mathrm{i}}$-CT, the total energy of the simulation is Gaussian distributed with about the same width (Fig. 3, orange and blue), confirming that energy does not drift significantly during the course of the 300 ps simulation time. Furthermore, since the cutoff r_{CT} is small, the extra computational cost is minor (≈5%) and scales linearly with the system size.

C. Anisotropic polarizability

For the TL4P$^{\mathrm{a1}}$-CT model, the polarizability tensor is set to the experimental anisotropic gas phase polarizability with $\alpha_{xx} = 1.468$ Å^3, $\alpha_{yy} = 1.415$ Å^3, and $\alpha_{zz} = 1.528$ Å^3, where x is the direction of the dipole moment axis, y is the axis perpendicular to the plane, and z is the direction from one hydrogen atom to the other.[71] We can separate that polarizability into two contributions:

$$\boldsymbol{\alpha} = \alpha_{\mathrm{iso}} \mathbf{1} + \boldsymbol{\alpha}_{\mathrm{aniso}}, \quad (4)$$

the isotropic polarizability α_{iso} and the traceless anisotropy tensor $\boldsymbol{\alpha}_{\mathrm{aniso}}$. We will see that the experimental anisotropy over-estimates the intensity of the 600 cm^{-1} band in the Raman spectrum [see Fig. 8(d)]. By linearly interpolating between the experimental anisotropic and isotropic polarizability $\alpha_{iso}\mathbf{1}$ as to correctly describe the intensity of the 600 cm^{-1} band, we get $\alpha_{xx} = 1.4692$, $\alpha_{yy} = 1.4427$, and $\alpha_{zz} = 1.4992$ Å^3, which has been used in the construction of the TL4P$^{\mathrm{a2}}$-CT model.

Also the addition of an anisotropic polarizability is computationally inexpensive (≈1.5%) and scales linearly with the number of water molecules. For the calculation of the forces, one has to account for the fact that the induced dipole moments are no longer parallel to the electric field and thus produce an additional torque that acts on the water molecule as a whole. By solving a system of linear equations, that torque is redistributed into forces acting on the atoms, which are calculated in such a way that the force on the center of mass, as well as the forces along the bonds, vanishes. As for the charge transfer, the correct implementation has been verified by testing the energy stability (Fig. 3, green).

D. Fitting procedure

In re-parametrizing the modified force fields TL4P$^{\mathrm{i}}$-CT, TL4P$^{\mathrm{a1}}$-CT, and TL4P$^{\mathrm{a2}}$-CT with the polarizabilities reported in Sec. III C, we stuck as closely as possible to the design philosophy of TL4P[50] and tried to modify its parameters as little as possible. That is, we retained the molecular geometry from TL4P ($r_{\mathrm{OH}} = 0.968$ Å and $\theta = 105.3°$) as well as the width of the Gaussian inducible dipoles ($\sigma = 0.842$ Å). Our initial intention has been to also keep the electrostatic parameters from TL4P ($q_{\mathrm{M}} = -1.1154\ e$, $q_{\mathrm{H}} = 0.5577\ e$, and $l_{\mathrm{OM}} = 0.2419$ Å, see Table I) in order to get a gas phase dipole moment of 1.855 D. However, the charge redistribution scheme of Fig. 2 enlarges the dipole moment of individual water molecules, and we found that it increases the electrostatic interactions too strongly. In order to compensate for the additional attracting forces, the static dipole moment had to be reduced by 2% (*vide infra*). We thus chose $q_{\mathrm{M}} = -1.0963\ e$ and $q_{\mathrm{H}} = 0.548\,15\ e$ for the charges and decided to keep $l_{\mathrm{OM}} = 0.2419$ Å. The static dipole moment then is $\mu^{\mathrm{stat}} = 1.818$ D.

After assigning q_{M}, q_{H}, l_{OM}, θ, $\boldsymbol{\alpha}$, and σ, the only free parameters determining the electrostatics of the model are the charge transfer parameters r_{CT} and q_{CT} from Eq. (3). Their values were optimized to give the best agreement of the dipole moment of small water clusters with dipole moments from DFT calculations, according to the following procedure. Using the TL4P force field, a 500 ps long MD trajectory was produced with coordinates saved in steps of 1 ps. One water molecule was randomly selected from each of these snapshots. For this water molecule, all neighbors were selected

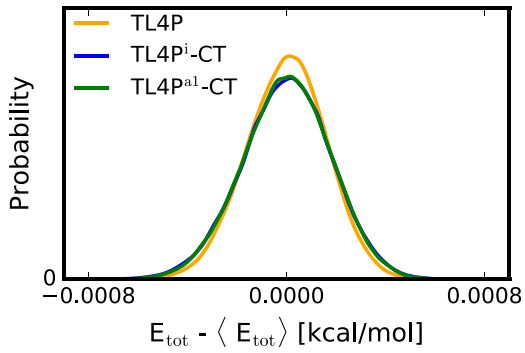

FIG. 3. Distribution of total energy per water molecule from *NVE* simulations with tight convergence criteria.

TABLE I. Force field parameters of the TL4P model and the newly developed charge transfer models.

Parameter	TL4P[50]	TL4P^{i}-CT	TL4P^{a1}-CT	TL4P^{a2}-CT
l_{OM} (Å)	0.2419	0.241 9	0.241 9	0.2419
θ (deg)	105.3	105.3	105.3	105.3
σ (Å)	0.842	0.842	0.842	0.842
α_{xx} (Å^3)	1.47	1.47	1.468	1.4692
α_{yy} (Å^3)	1.47	1.47	1.415	1.4427
α_{zz} (Å^3)	1.47	1.47	1.528	1.4992
q_M (e)	−1.1154	−1.096 3	−1.096 3	−1.0963
q_H (e)	0.5577	0.548 15	0.548 15	0.4815
q_{CT} (e)	...	0.052 9	0.052 9	0.0529
r_{CT} (Å)	...	2.813	2.813	2.813
A_1 (kcal/mol)	84 120	191 600	196 150	192 300
A_2 (Å^{-1})	3.55	3.801 6	3.810 1	2.8032
B (Å^6 kcal/mol)	992	1000.7	1000.7	1000.7

with a O–O distance smaller than 3.5 Å. In this way, 500 water clusters consisting of 4 to 9 water molecules were generated.

The total dipole moments $\boldsymbol{M}_i^{QM}$ of all clusters i were calculated with the help of DFT calculations (see Sec. II for details). For the sake of calculating the corresponding dipole moments $\boldsymbol{M}_i^{MM}$ of the various molecular mechanics (MM) water models and comparing them to $\boldsymbol{M}_i^{QM}$, the charges and polarizabilities of the former had to be slightly modified in order to reflect the gas phase dipole moment and polarizability of DFT water. The values calculated are μ^{DFT} = 1.805 D for the dipole moment and α_{xx}^{DFT} = 1.542 Å^3, α_{yy}^{DFT} = 1.504 Å^3, and α_{zz}^{DFT} = 1.591 Å^3 for the polarizability. The root mean square deviation (RMSD) between $\boldsymbol{M}_i^{QM}$ and $\boldsymbol{M}_i^{MM}(q_{CT}, r_{CT})$, averaged over all clusters, has then been calculated as a function of charge transfer parameters. Minimizing the RMSD reveals q_{CT} = 0.0529 e and r_{CT} = 2.813 Å for TL4P^{i}-CT; see Fig. 4(a). We chose to use that set of parameters for all water models, isotropic and anisotropic.

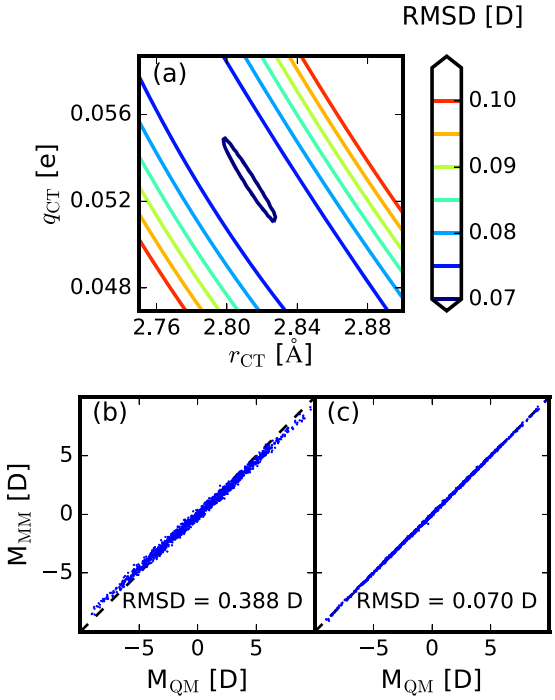

FIG. 4. (a) RMSD of TL4P^{a}-CT *versus* DFT as a function of r_{CT} and q_{CT}. Correlation of the dipole moment of the 500 test clusters calculated (b) for TL4P and (c) for TL4P^{a}-CT *versus* DFT, plotting the x, y, and z components of the dipole moments individually.

Modifying the electrostatic parameters changes the interactions between water molecules, which requires to reparametrize the van der Waals parameters A_1, A_2, and B [Eq. (2)]. As done for TL4P,[50] we fitted them to the position of the first peak in the O–O radial distribution function, the pressure (p = 1 bar), and the average potential energy per water molecule ($\langle E_{pot} \rangle$ = −9.92 kcal/mol). The target of the position of the first peak in the O–O radial distribution function has been a little larger (r_{max} = 2.8 Å) than for TL4P, as this is the best accepted experimental value.[73] The slight adjustment of the static charges q_M and q_H, reducing the static dipole by 2% relative to that of TL4P, has been necessary to find a set of van der Waals parameters that reproduce all target values r_{max}, E_{pot}, and p at the same time. All parameters are summarized in Table I, where they are also compared to TL4P.

IV. MODEL VERIFICATION

A. Electrostatics

The dipole moments calculated from the fitted models are in excellent agreement with DFT dipole moments with an RMSD of only 0.070 D, which is 5.5 times smaller than the RMSD calculated for TL4P [Figs. 4(b) and 4(c)]. Adding charge transfer improves the correlation not only for small dipole moments but also for high dipole moments around −10 D or 10 D [see Fig. 4(c)]. Although more data points exist from smaller clusters with smaller dipole moments, the model has good quality also for higher values of the dipole moments arising from the bigger clusters. This observation supports the conclusion that including charge transfer across hydrogen bonds improves the dipole moment surface for the right physical reason.

For a hydrogen bonded water dimer with an H···M distance of 1.85 Å, the amount of charge transferred is 0.025 e, which is consistent with values reported from various QM calculations at different levels of theory ranging from HF to MP2.[52–55,57] A water molecule in a liquid water box, on the other hand, is neutral in average, but its charge fluctuates with a standard deviation of 0.013 e [Fig. 5(a)]. The average dipole increases from 2.48 D to 2.52 D when going from TL4P to TL4P^{i}-CT [Fig. 5(b)], despite the fact that the dipole of the corresponding gas-phase monomers had been reduced from 1.855 D to 1.818 D. Furthermore, the fluctuation amplitude of the dipole moment slightly increases from 0.136 D to 0.150 D.

B. Thermodynamic and structural properties

In the following, various experimental observables were calculated for the new water models, based on similar techniques as those used to characterize the original TL4P model.[50] We start with the dielectric constant,[74]

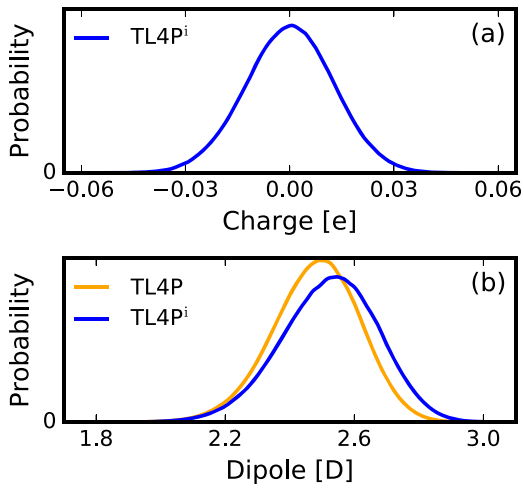

FIG. 5. (a) Molecular charge distribution of a TL4P^{i}-CT water molecule in liquid water and (b) molecular dipole moment distribution of TL4P and TL4P^{i}-CT. Since the water molecules are charged in the case of TL4P^{i}-CT, the dipole moment depends on the choice of a reference point. We chose the geometrical midpoint of the charged sites (i.e., H and M sites) as a reference point, which is equivalent to subtracting the net charge evenly from these sites.

$$\epsilon_{\mathrm{rel}} = \frac{1 + \frac{\langle \boldsymbol{M}^2\rangle - \langle \boldsymbol{M}\rangle^2}{3\epsilon_0 V k_B T}\frac{2\epsilon_{\mathrm{RF}}}{2\epsilon_{\mathrm{RF}}+1}}{1 - \frac{\langle \boldsymbol{M}^2\rangle - \langle \boldsymbol{M}\rangle^2}{3\epsilon_0 V k_B T}\frac{1}{2\epsilon_{\mathrm{RF}}+1}}. \tag{5}$$

Here, the standard deviation of the total dipole moment has been averaged during ∼45 ns, initially in an environment with the experimental dielectric constant $\epsilon_{\mathrm{RF}} = 78$. The dielectric constant has then been iterated self-consistently until $\epsilon_{\mathrm{rel}} \approx \epsilon_{\mathrm{RF}}$ within the uncertainty of the calculation.

The isothermal compressibility κ_T,[75] the thermal expansion coefficient α_p,[76] and the heat capacity c_p, all at $T = 300$ K and experimental density $\rho = 0.9965$, were derived from numerical differentiation, varying ρ by ±0.0015 g/cm^3 and T by ±5 K,

$$\kappa_T = \left.\frac{\partial \ln \rho}{\partial p}\right|_T, \tag{6}$$

$$\alpha_p = -\left.\frac{\partial \ln \rho}{\partial T}\right|_p, \tag{7}$$

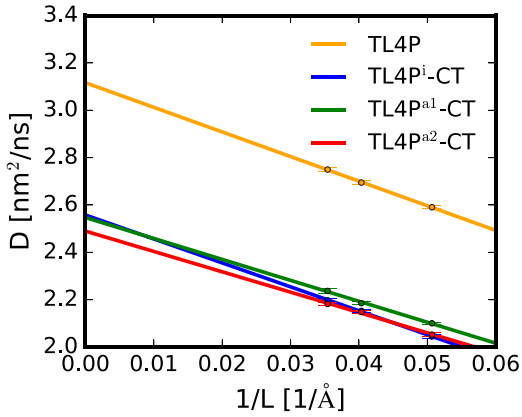

FIG. 6. Box-size dependent diffusion constant plotted against $1/L$, where L is the box size, together with linear fits used to extract the size-corrected diffusion constant D_0 and the viscosity η.

$$c_p = \left.\frac{\partial E_{\mathrm{tot}}}{\partial T}\right|_p + \Delta C_{\mathrm{QM}}, \tag{8}$$

where $\Delta C_{\mathrm{QM}} = -2.22$ cal mol^{-1} K^{-1} is a correction for quantum mechanical contributions (from internal degrees of freedom, as well as quantum mechanical character of the libration) to the heat capacity.[77]

The diffusion coefficient was calculated from

$$D = \frac{1}{6}\left.\frac{dc(t)}{dt}\right|_{t=t_0}, \tag{9}$$

at $t_0 = 90$ ps by numeric differentiation. The autocorrelation function $c(t) = \left\langle (\boldsymbol{r}(t) - \boldsymbol{r}(0))^2 \right\rangle$ was averaged over a simulation time of 27 ns. Size-dependent diffusion constants were calculated in that way for boxes containing 256, 507, and 750 water molecules. From these results, the size-corrected diffusion constant D_0 and viscosity η were extracted by utilizing the relationship[78,79]

$$D = D_0 - \frac{k_B T \zeta}{6\pi\eta V^{1/3}}, \tag{10}$$

where V is the volume of the simulation box and $\zeta \approx 2.837$ is a constant originating from the Ewald summation in a cubic periodic box. A linear fit of the size-dependent diffusion constant as a function of $1/L = 1/V^{1/3}$ reveals D_0 from the intercept and the viscosity η from the slope [Fig. 6].

TABLE II. All observables calculated for the new water molecules, compared to experiment and values obtained from TL4P, at 300 K and a density of 0.9965 g cm^{-3}. In the case of TL4P, the results reported in Ref. 50 are given (6th column) together with those calculated with exactly the same procedures as for the new models (5th column) for better comparison (both sets of numbers differ slightly since the electrostatic interactions were calculated differently in Ref. 50, and since we applied a long-range correction for the van der Waals potential).

	TL4P^{i}-CT	TL4P^{a1}-CT	TL4P^{a2}-CT	TL4P	TL4P[50]	Expt.
$r_{\max}$ (Å)	2.80 ± 0.01	2.80	2.80 ± 0.01	2.77 ± 0.01	2.76	2.80[73]
E_{pot} (kcal/mol)	−9.9199 ± 0.0007	−9.923 ± 0.001	−9.9230 ± 0.0001	−9.9580 ± 0.0005	−9.92	−9.92[72]
p (bar)	−14 ± 3	−26 ± 2	−25 ± 2	−168 ± 2	1	1[80]
ϵ_{rel}	86 ± 2	84 ± 3	85 ± 3	69 ± 3	77	78[81]
D_0 (nm^2/ns)	2.49 ± 0.02	2.56 ± 0.02	2.55 ± 0.02	3.12 ± 0.01	3.0	2.4[82]
η (mPa s)	0.64 ± 0.03	0.70 ± 0.04	0.73 ± 0.05	0.60 ± 0.01	0.80	0.81[83]
α_p (10^{-4}/K)	6.4 ± 0.2	6.4 ± 0.2	6.4 ± 0.2	6.1 ± 0.1	5.9	2.8[84]
κ_T (10^{-6}/atm)	35 ± 2	42 ± 2	37 ± 2	39 ± 2	37.4	45.6[84]
c_p [cal/(mol K)]	20.5 ± 0.1	20.3 ± 0.1	20.4 ± 0.1	18.9 ± 0.1	18.7	18.0

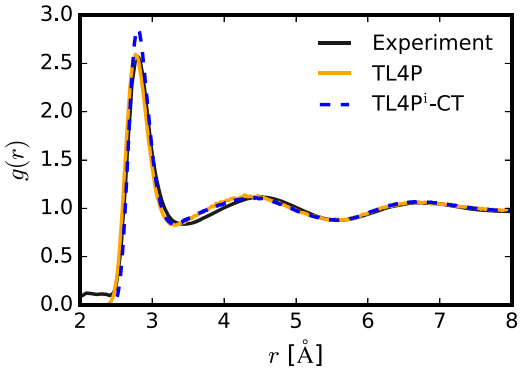

FIG. 7. RDF of TL4P and TL4P^{i}-CT compared to the experimental RDF.[73] The RDFs of TL4P^{a1}-CT and TL4P^{a2}-CT are virtually the same as that of TL4P^{i}-CT and are not shown.

The results of all these calculations are summarized in Table II. Finally, Fig. 7 shows the O–O radial distribution functions.

Generally speaking, anisotropic polarizability does barely affect the thermodynamic and structural properties of the force field, which is why we restrict the discussion to a comparison of TL4P with TL4P^{i}-CT. The O–O RDF (Fig. 7) of the fitted models has a first peak at 2.80 Å (by construct) with a height of 2.82, which is higher than that of TL4P (2.59), and also higher than the experimental value (2.57).[73] At distances larger than 3.5 Å, the RDFs from TL4P and TL4P^{i}-CT are almost identical. The similar long-range structuring is attributed to the same long-range electrostatic interactions, when charge transfer no longer plays any significant role. Compared to the experimental RDF, however, the second peak is shifted to shorter distances (4.29 Å *versus* 4.45 Å, respectively), indicating that both models underestimate the tetrahedrality of the second solvation layer. On the other hand, the height of minima and maxima after the first peak agrees well with experiment.

The calculated values for the pressure and potential energy for TL4P are $p = -168$ bars and $E_{\text{pot}} = -9.958$ kcal/mol, lower than the values reported by Tavan and co-workers.[50] This reflects the different treatment of electrostatic long-range interactions, as well as the long-range correction to the van der Waals potential that we applied here. Since it has been a fitting target, the corresponding numbers agree well with experiment for all models TL4P^{i}-CT, TL4P^{a1}-CT, and TL4P^{a2}-CT. The thermal expansion coefficient α_p increases slightly from $6.1\cdot10^{-4}$ to $6.4\cdot10^{-4}$ K^{-1} upon addition of charge transfer. This is more than double the experimental value of $2.8\cdot10^{-4}$ K^{-1}[84] and reflects the failure of TL4P, as well as of all our new models, to correctly describe the density maximum of water at 4 °C and is considered to be a major drawback of all these models. The isothermal compressibility stays the same within the uncertainty of the calculation. The heat capacity increases from 18.9 to 20.5 cal mol^{-1} K^{-1}, while the dielectric constant increases from 69 to 86.

Concerning dynamical properties, we observe that the diffusion constant D_0 decreases from 3.1 to 2.5 nm^2/ns, while the viscosity increases from 0.60 ± 0.01 to 0.64 ± 0.03 mPa s in TL4P^{i}-CT and further to 0.73 ± 0.05 mPa s in TL4P^{a2}-CT.

V. SPECTRA

A. Vibrational density of states

To obtain a basis for discussing differences between water models in the THz and Raman spectra, we first consider the vibrational density of states (VDOS), which is related to the dynamics only and thus can be used to disentangle effects of dynamics from the electronic contributions to the spectra, i.e., the transition dipoles and transition polarizabilities. The VDOS has been calculated from the velocity autocorrelation function of either the oxygen or the hydrogen atoms,

$$\text{VDOS}_{\text{O,H}}(\omega) = \text{Re}\int_0^\infty dt e^{i\omega t}\langle \boldsymbol{v}_{\text{O,H}}(0)\cdot\boldsymbol{v}_{\text{O,H}}(t)\rangle, \quad (11)$$

where the velocity autocorrelation function has been apodized at 4 ps and $\langle\ldots\rangle$ denotes an ensemble average as well as a time average, the latter over a 1.5 ns long trajectory. In the VDOS of the hydrogen atoms [VDOS_{H}, see Fig. 8(b)], the three bands corresponding to hydrogen bond bending, hydrogen bond vibration, and libration are present. By contrast, the 600 cm^{-1} band is absent in VDOS_{O} [Fig. 8(a)], which shows that librations are dominated by motions of the hydrogen atoms [Fig. 1(a)]. Upon addition of charge transfer, the 200 cm^{-1} and the 600 cm^{-1} bands are shifted slightly toward higher frequencies, indicating a somewhat stronger hydrogen bonding, while the amplitude of the hydrogen-bond vibration at 200 cm^{-1} is reduced somewhat [Fig. 8(a), orange *versus* blue line]. For both the oxygen and the hydrogen VDOS, addition of anisotropic polarizability has no visible effect [see the red dashed line in Figs. 8(a) and 8(b) for TL4P^{a2}-CT; the result for TL4P^{a1}-CT is virtually identical and is not shown].

B. THz absorption spectrum

The THz absorption spectrum [Fig. 8(c)] has been calculated from the dipole-dipole autocorrelation function,[85]

$$I_{\text{THz}}(\omega)n(\omega) \propto \tanh\left(\frac{\beta\hbar\omega}{2}\right)\text{Im}\int_0^\infty dt\, e^{i\omega t}\langle\boldsymbol{\mu}(t)\cdot\dot{\boldsymbol{\mu}}(0)\rangle, \quad (12)$$

where the dipole autocorrelation function has been apodized at 4 ps, $\langle\ldots\rangle$ denotes a time average over a 7 ns long trajectory, $n(\omega)$ is the experimental refractive index, and $\tanh(\beta\hbar\omega/2)$ is a quantum correction factor.[86] The dipole moment $\boldsymbol{\mu}(t)$ of the simulation box as a whole has contributions from the static charges q_i, the induced dipole moments due to polarizability $\boldsymbol{\mu}_i$, and from charge transfer δq_i. The latter renders the water-molecules non-neutral, which calls for care when calculating the dipole moment in connection with the periodic boundary conditions; one cannot simply sum over all charges including the charge transfers $\boldsymbol{\mu} = \sum_i \boldsymbol{\mu}_i + \boldsymbol{r}_i(q_i + \delta q_i)$. In order to circumvent that problem, we calculated the contribution of charge transfer to the overall dipole independent from the other two contributions (which are not problematic). If two waters in a hydrogen-bonded dimer are in different image boxes, the minimum image convention is used for the calculation of the dipole that originates from the charge transfer across that dimer.

The THz absorption spectrum of TL4P almost completely lacks the band at 200 cm^{-1} [Fig. 8(c), orange line]. As

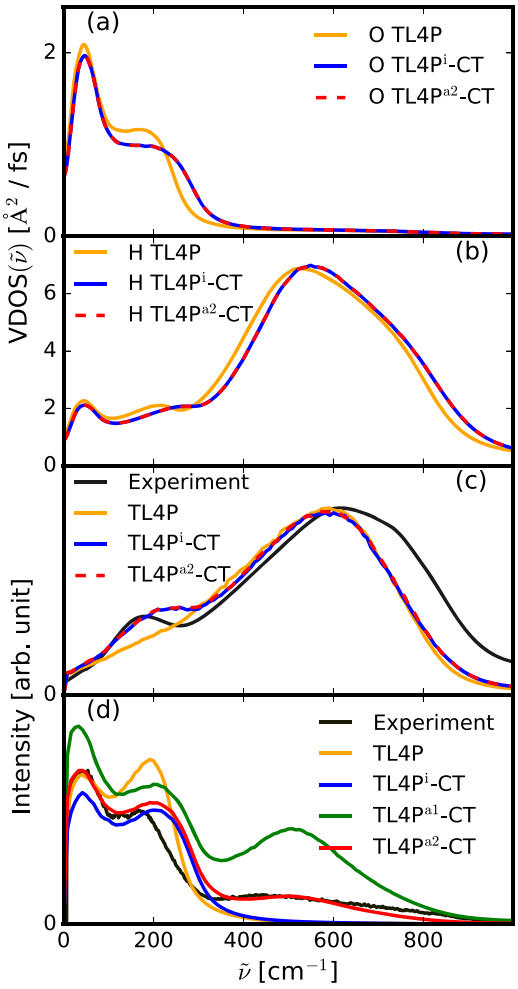

FIG. 8. (a) Vibrational density of states of the O-atoms and (b) the H-atoms, (c) THz absorption spectra, and (d) anisotropic Raman spectra. Experimental data are shown in black [panels (c) and (d)],[13,14] while the simulation results for TL4P are shown in orange, TL4P^{i}-CT in blue, TL4P^{a1}-CT in green, and TL4P^{a2}-CT in red. In some cases [panels (a)–(c)], the models with anisotropic polarizability are virtually indistinguishable from TL4P^{i}-CT, in which case TL4P^{a1}-CT is not shown and TL4P^{a2}-CT is shown as the red dashed line [panel (a)–(c)]. While the experimental spectrum has been scaled to the simulated ones with an arbitrary factor in panels (c) and (d), the scaling of the spectra of the various water models among each other is absolute and the intensities of the various peaks can be compared directly.

anticipated by the work of Torii,[58] that band appears by adding charge transfer [Fig. 8(c), blue line]. Comparison with the VDOS [Fig. 8(a)] emphasizes that this effect is not due to modified nuclear dynamics; rather it reflects the fact that charge transfer gives that vibration a transition dipole. Its intensity, measured relative to that of the 600 cm^{-1} band, agrees reasonably with experiment. The intensity and position of the 600 cm^{-1} band, on the other hand, are not affected by charge transfer. Going from isotropic to anisotropic polarizability has no effect on the absorption spectrum; the absorption spectra of TL4P^{i}-CT, TL4P^{a1}-CT, and TL4P^{a2}-CT are virtually the same. The librational band of all water models (including TL4P) is at slightly lower frequency than in the experimental spectrum (590 cm^{-1} *versus* 620 cm^{-1}). A similarly shifted frequency is commonly observed for various rigid four point water models[20,43] and might originate from underestimating the orientational confinement due to the simplicity of the electrostatics of these four point models or due to the use of only one van der Waals site on the oxygen. Conversely, the hydrogen bond stretching mode around 200 cm^{-1} is at slightly too high frequency in all water models using charge transfer, an effect that is also seen in the VDOS. This indicates that the force fields somewhat overestimate the hydrogen-bond strength, probably for the same reason as the too large amplitude of the first peak in the RDF (Fig. 7). A Gaussian distribution for the point charges (and not only the induced dipoles) might also be a way to further improve the model.

C. Anisotropic Raman spectrum

The anisotropic Raman spectrum [Fig. 8(d)] was calculated from the polarizability-polarizability autocorrelation function,[85]

$$I^{ani}_{\text{Raman}}(\omega) \propto \text{Im} \int_0^\infty dt e^{i\omega t} \left\langle \text{tr}\left[\mathbf{\Pi}^{ani}(t) \cdot \dot{\mathbf{\Pi}}^{ani}(0)\right]\right\rangle \tag{13}$$

with

$$\mathbf{\Pi}^{ani} = \mathbf{\Pi} - 3\text{tr}[\mathbf{\Pi}]\mathbf{1}. \tag{14}$$

Here, the instantaneous polarizability $\mathbf{\Pi}(t)$ of the simulation box as a whole is

$$\mathbf{\Pi}(t) = \frac{\partial \boldsymbol{\mu}(t)}{\partial \boldsymbol{E}_{ext}}, \tag{15}$$

which is calculated by numerical differentiation with respect to an external field $\boldsymbol{E}_{ext}$, varying it by $\pm 0.003\ e/\text{Å}^2$.

Adding charge transfer to TL4P with isotropic polarizability (i.e., TL4P^{i}-CT) slightly increases the frequency of the 200 cm^{-1} band [Fig. 8(d)], as already seen in the VDOS [Figs. 8(a) and 8(b)]. At the same time, the intensities of both the 50 cm^{-1} and 200 cm^{-1} bands are reduced [Fig. 8(d) blue *versus* orange line], with the effect being more pronounced for the 200 cm^{-1} band. Since the effect of inter-molecular fields and an external field is additive, adding charge transfer according to Eq. (3) does not affect the polarizability of the simulation box as a whole if the geometry would be the same. That is, if one takes the derivative Eq. (15) of Eq. (1),

$$\mathbf{\Pi}(t) = \sum_{i \neq j} \boldsymbol{\alpha}_i \left(\mathbf{1} + \boldsymbol{T}_{ij}\boldsymbol{\alpha}_j\right), \tag{16}$$

the result is a complicated function of structure (via $\boldsymbol{T}_{ij}$ and the fact that the $\boldsymbol{\alpha}_i$ need to be rotated into the laboratory frame), but the contribution of $\boldsymbol{E}_j$ disappears, which is where charge transfer enters. As such, the change in the Raman spectrum originates from structural or dynamical differences between the TL4P and the TL4P^{i}-CT models. The reduction of the intensity is however more than what would be expected from the decreased VDOS at 200 cm^{-1} [Fig. 8(d)].

Again as anticipated, including anisotropic polarizability in TL4P^{a1}-CT and TL4P^{a2}-CT, the librational mode around 600 cm^{-1} [Fig. 8(d), red and green line] obtains transition polarizability. When using the experimental anisotropic polarizability tensor[71] in TL4P^{a1}-CT, its intensity is overestimated [Fig. 8(d), green line], which is why we linearly interpolated in TL4P^{a2}-CT between the experimental anisotropic polarizability and an isotropic polarizability as to match the relative intensities of the 600 cm^{-1} and 200 cm^{-1} bands [Fig. 8(d), red line]. We find that the intensity of the

600 cm^{-1} band scales roughly quadratically with the anisotropy of the polarizability tensor α_{aniso} [defined in Eq. (4)]. Interestingly, addition of an anisotropic polarizability regains intensity for the 50 cm^{-1} band, despite the fact that the VDOS is practically identical [Figs. 8(a) and 8(b), red *versus* blue line]. In contrast to the hydrogen bond stretch vibration, the hydrogen bond bending modes include a rotation of water molecules, giving that mode additional transition polarizability; hence the intensity of the 50 cm^{-1} band is affected more by including anisotropic polarizability than the 200 cm^{-1} band.

VI. CONCLUSION AND OUTLOOK

In conclusion, we have amended the TL4P model of Tavan and co-workers[50] with charge transfer and an anisotropic polarizability, using a mixed quantum-chemical/empirical approach. The goal has been to correctly describe both the THz absorption and the Raman spectrum in a frequency range 0–1000 cm^{-1}, where the intermolecular modes of water are found. While the addition of charge transfer required a reparametrization of the van der Waals parameters, despite the fact that the average amount of charge transfer is small (0.025 *e*), the small anisotropic correction of the polarizability did not further affect the thermodynamic properties of the model. In parametrizing the models, we tried to only minimally change the parameters of the original TL4P model, and we were furthermore guided by the design philosophy of TL4P,[50] namely, that the dipole moment and polarizability of a water monomer should reflect the experimental gas phase value. We had to compromise on two points, i.e., reduce the dipole moment by 2% relative to the experimental value and fit the anisotropy of the polarizability as to match the experimental intensity of the librational mode. Considering the simplicity of the charge transfer model, the improvement of the dipole moment of small water clusters upon the addition of charge transfer is quite remarkable (Fig. 4).

The thermodynamic properties are of equal quality as those of TL4P with an overall good agreement with experiment (see Table II; the thermal compressibility and consequently also the density maximum are an exception to that statement). On the other hand, the diffusion constant and viscosity decrease/increase to a value much closer to experiment. The water force fields developed using the design principle of TL4P generally tend to overestimate the diffusion constant, and charge transfer seems to be a good way to slow down the motions without greatly affecting the thermodynamics. This observation probably reflects the fact that charge transfer strengthens the directional hydrogen bonds on the expense of the isotropic van der Waals interactions.

Concerning the inter-molecular THz absorption and Raman spectra, the final result of TL4P^{a2}-CT reveals an almost perfect agreement with experiment, in particular with regard to the relative intensities of the various contributions [Figs. 8(c) and 8(d), red *versus* black line]. We use one set of electrostatic parameters for the calculation of both the forces in the MD simulation and the dipole moments for the calculation of the THz and Raman spectra; hence both are calculated in a self-consistent way. One might argue that the potential energy surface and dipole moment surface might be better described by independently optimized functions. For example, point charge models tend to use "effective charges," which are designed to mimic the intermolecular forces but do not necessarily reflect the real charge distribution of the system, the latter of which determines the spectroscopy. If a force field has only few degrees of freedom, trying to fit the potential energy surface and dipole moment surface simultaneously will decrease the quality of the force field because compromises will have to be made. On the other hand, once one is using an *ab initio* derived electrostatic function together with polarizability and is in addition adjusting it to THz absorption and Raman spectra, which measure the dynamics of those charges very directly; one should be able to represent the real charge distribution quite realistically. In this regard, one should also keep in mind that Coulomb interactions are long-ranged. As such charge transfer effects, which manifest themselves in the THz absorption spectrum, must have consequences on the structure of water even on larger distances. The changes in the VDOS and Raman spectra emphasize that this is indeed the case. We are convinced that the mixed quantum chemical/empirical approach for fitting the TL4P models together with their physically motivated cornerstones can lead to very transferrable water force fields.

The present work also illustrates that force field refinement by fitting to reference spectroscopic data is a powerful way to improve empirical energy functions. This is because the experimentally determined spectroscopic features directly probe the dynamics, and thereby intermolecular interactions, on time scales relevant to molecular motions. Approaches similar in spirit to the present work have been applied for example to improved energy functions for understanding the proton transfer dynamics in small molecules.[87,88]

Our primary motivation for developing these water models is the modeling of 2D-Raman-THz spectroscopy.[16] An obvious prerequisite for that purpose is a model that correctly describes the (1D) THz absorption and Raman spectra,[43] which we now have at our hands with TL4P^{a2}-CT. But the series of models, TL4P, TL4P^{i}-CT, and TL4P^{a2}-CT, offers an additional avenue via the possibility to switch on and off the 200 cm^{-1} (THz) and the 600 cm^{-1} bands (Raman) at wish. Assigning spectroscopic features in 2D-Raman-THz spectra is a cumbersome task since they strongly overlap and a calculation based on a full-atom MD simulation is largely black-box. Being able to switch on and off certain bands will greatly facilitate the assignment of diagonal and in particular cross peaks in the 2D-Raman-THz spectrum of water. Work in this direction is currently ongoing.

But more generally speaking, we think of 2D-Raman-THz spectroscopy as a spectroscopic method that is extremely sensitive to the accuracy, with which one describes the polarizability of a water model.[20] While a point charge model such as TIP4P/2005 with its average polarization probably describes the structure of bulk water quite well,[89] it must fail at least to a certain extent once water comes into contact with, e.g., the hydrophobic surface of a protein since its polarization and hence Coulombic interactions will be different. Only a polarizable force can describe that situation correctly, and the information about polarizability is encoded in 1D THz and

Raman spectra, and even more so in 2D-Raman-THz spectra. At the same time, a polarizable water force field needs to be computationally inexpensive in order to be competitive for biomolecular simulations. This calls for a rigid water model, in which case one can then take advantage of a longer integration time step of typically 2 fs. The additional computational cost for charge transfer and the anisotropic polarizability is minor. We wish to advocate TL4P^{a2}-CT as a computationally very efficient force field with a very good polarizability function.

SUPPLEMENTARY MATERIAL

See supplementary material for the complete source code, two different water boxes as initial conditions, and a brief tutorial describing its compilation and usage.

ACKNOWLEDGMENTS

The work has been supported by the Swiss National Science Foundation (SNF) through the NCCR MUST.

[1] I. Brovchenko and A. Oleinikova, ChemPhysChem **9**, 2660 (2008).
[2] P. G. Debenedetti, J. Phys.: Condens. Matter **15**, R1669 (2003).
[3] S. Yeremenko, M. S. Pshenichnikov, and D. A. Wiersma, Chem. Phys. Lett. **369**, 107 (2003).
[4] J. B. Asbury, T. Steinel, K. Kwak, S. A. Corcelli, C. P. Lawrence, J. L. Skinner, and M. D. Fayer, J. Chem. Phys. **121**, 12431 (2004).
[5] J. D. Eaves, J. J. Loparo, C. J. Fecko, S. T. Roberts, A. Tokmakoff, and P. L. Geissler, Proc. Natl. Acad. Sci. U. S. A. **102**, 13019 (2005).
[6] M. L. Cowan, B. D. Bruner, N. Huse, J. R. Dwyer, B. Chugh, E. T. J. Nibbering, T. Elsaesser, and R. J. D. Miller, Nature **434**, 199 (2005).
[7] A. Tokmakoff, Acc. Chem. Res. **42**, 1239 (2009).
[8] F. Perakis and P. Hamm, J. Phys. Chem. B **115**, 5289 (2011).
[9] R. A. Nicodemus, S. A. Corcelli, J. L. Skinner, and A. Tokmakoff, J. Phys. Chem. B **115**, 5604 (2011).
[10] K. Ramasesha, L. De Marco, A. Mandal, and A. Tokmakoff, Nat. Chem. **5**, 935 (2013).
[11] M. Heyden, J. Sun, S. Funkner, G. Mathias, H. Forbert, M. Havenith, and D. Marx, Proc. Natl. Acad. Sci. U. S. A. **107**, 12068 (2010).
[12] F. N. Keutsch and R. J. Saykally, Proc. Natl. Acad. Sci. U. S. A. **98**, 10533 (2001).
[13] J. E. Bertie and Z. Lan, Appl. Spectrosc. **50**, 1047 (1996).
[14] E. W. Castner, Y. J. Chang, Y. C. Chu, and G. E. Walrafen, J. Chem. Phys. **102**, 653 (1995).
[15] P. Hamm and A. Shalit, J. Chem. Phys. **146**, 130901 (2017).
[16] J. Savolainen, S. Ahmed, and P. Hamm, Proc. Natl. Acad. Sci. U. S. A. **110**, 20402 (2013).
[17] A. Shalit, S. Ahmed, J. Savolainen, and P. Hamm, Nat. Chem. **9**, 273 (2017).
[18] S. Palese, J. T. Buontempo, L. Schilling, W. T. Lotshaw, Y. Tanimura, S. Mukamel, and R. J. Miller, J. Phys. Chem. **98**, 12466 (1994).
[19] S. Saito and I. Ohmine, J. Chem. Phys. **108**, 240 (1998).
[20] P. Hamm, J. Chem. Phys. **141**, 184201 (2014).
[21] M. W. Lee, J. K. Carr, M. Göllner, P. Hamm, and M. Meuwly, J. Chem. Phys. **139**, 054506 (2013).
[22] G. Lamoureux, A. D. MacKerell, and B. Roux, J. Chem. Phys. **119**, 5185 (2003).
[23] G. Lamoureux and B. Roux, J. Chem. Phys. **119**, 3025 (2003).
[24] G. Lamoureux, E. Harder, I. V. Vorobyov, B. Roux, and A. D. MacKerell, Chem. Phys. Lett. **418**, 245 (2006).
[25] P. T. Kiss and A. Baranyai, J. Chem. Phys. **138**, 204507 (2013).
[26] W. Yu, P. E. M. Lopes, B. Roux, A. D. Mackerell, W. Yu, P. E. M. Lopes, B. Roux, and A. D. Mackerell, J. Chem. Phys. **138**, 034508 (2013).
[27] S. W. Rick, J. Comput. Chem. **37**, 2060 (2016).
[28] A. J. Stone, Science **315**, 1228 (2007).
[29] J. Liu, W. H. Miller, G. S. Fanourgakis, S. S. Xantheas, S. Imoto, and S. Saito, J. Chem. Phys. **135**, 244503 (2011).
[30] V. Babin, G. R. Medders, and F. Paesani, J. Phys. Chem. Lett. **3**, 3765 (2012).
[31] C. J. Tainter, P. A. Pieniazek, Y. S. Lin, and J. L. Skinner, J. Chem. Phys. **134**, 184501 (2011).
[32] C. J. Tainter, L. Shi, and J. L. Skinner, J. Chem. Theory Comput. **11**, 2268 (2015).
[33] S. W. Rick, S. J. Stuart, and B. J. Berne, J. Chem. Phys. **101**, 6141 (1994).
[34] H. A. Stern, F. Rittner, B. J. Berne, and R. A. Friesner, J. Chem. Phys. **115**, 2237 (2001).
[35] P. Ahlström, A. Wallqvist, S. Engström, and B. Jönsson, Mol. Phys. **68**, 563 (1989).
[36] D. N. Bernardo, Y. Ding, K. Krogh-Jespersen, and R. M. Levy, J. Phys. Chem. **98**, 4180 (1994).
[37] L. X. Dang and T.-M. Chang, J. Chem. Phys. **106**, 8149 (1997).
[38] P. Ren and J. W. Ponder, J. Phys. Chem. B **107**, 5933 (2003).
[39] P. Paricaud, M. Předota, A. A. Chialvo, and P. T. Cummings, J. Chem. Phys. **122**, 244511 (2005).
[40] G. S. Fanourgakis and S. S. Xantheas, J. Chem. Phys. **128**, 074506 (2008).
[41] T. Hasegawa and Y. Tanimura, J. Phys. Chem. B **115**, 5545 (2011).
[42] M. L. Laury, L. P. Wang, V. S. Pande, T. Head-Gordon, and J. W. Ponder, J. Phys. Chem. B **119**, 9423 (2015).
[43] H. Ito, T. Hasegawa, and Y. Tanimura, J. Phys. Chem. Lett. **7**, 4147 (2016).
[44] M. Schwörer, C. Wichmann, P. Tavan, M. Schwörer, C. Wichmann, and P. Tavan, J. Chem. Phys. **144**, 114504 (2016).
[45] L.-P. Wang, T. Head-Gordon, J. W. Ponder, P. Ren, J. D. Chodera, P. K. Eastman, T. J. Martinez, and V. S. Pande, J. Phys. Chem. B **117**, 9956 (2013).
[46] R. Qi, L.-P. Wang, Q. Wang, V. S. Pande, and P. Ren, J. Phys. Chem. B **143**, 014504 (2015).
[47] B. T. Thole, Chem. Phys. **59**, 341 (1981).
[48] D. Elking, T. O. M. Darden, R. J. Woods, T. Park, and N. Carolina, J. Comput. Chem. **28**, 1261 (2007).
[49] T. M. Nymand and P. Linse, J. Chem. Phys. **112**, 6152 (2000).
[50] P. Tröster, K. Lorenzen, M. Schwörer, and P. Tavan, J. Phys. Chem. B **117**, 9486 (2013).
[51] J. L. Abascal and C. Vega, J. Chem. Phys. **123**, 234505 (2005).
[52] P.-O. Åstrand, K. Ruud, K. V. Mikkelsen, and T. Helgaker, J. Phys. Chem. A **102**, 7686 (1998).
[53] J. Korchowiec and T. Uchimaru, J. Chem. Phys. **112**, 1623 (2000).
[54] O. Gálvez, P. C. Gómez, and L. F. Pacios, J. Chem. Phys. **115**, 11166 (2001).
[55] E. D. Glendening, J. Phys. Chem. A **109**, 11936 (2005).
[56] R. Kumar, J. R. Schmidt, and J. L. Skinner, J. Chem. Phys. **126**, 204107 (2007).
[57] R. Z. Khaliullin, A. T. Bell, and M. Head-Gordon, Chem. - Eur. J. **15**, 851 (2009).
[58] H. Torii, J. Chem. Theory Comput. **10**, 1219 (2014).
[59] A. J. Lee and S. W. Rick, J. Chem. Phys. **134**, 184507 (2011).
[60] T. A. Kesselring, E. Lascaris, G. Franzese, S. V. Buldyrev, H. J. Herrmann, and H. E. Stanley, J. Chem. Phys. **138**, 244506 (2013).
[61] W. C. Swope, H. C. Andersen, P. H. Berens, and K. R. Wilson, J. Chem. Phys. **76**, 637 (1982).
[62] V. Kräutler, W. F. Van Gunsteren, and P. H. Hünenberger, J. Comput. Chem. **22**, 501 (2001).
[63] G. Bussi, D. Donadio, and M. Parrinello, J. Chem. Phys. **126**, 014101 (2007).
[64] H. Bekker, E. J. Dijkstra, M. K. R. Renardus, and H. J. C. Berendsen, Mol. Simul. **14**, 137 (1995).
[65] J. Hutter, M. Iannuzzi, F. Schiffmann, and J. Vandevondele, Wiley Interdiscip. Rev.: Comput. Mol. Sci. **4**, 15 (2014).
[66] J. VandeVondele and J. Hutter, J. Chem. Phys. **118**, 4365 (2003).
[67] J. P. Perdew, K. Burke, and M. Ernzerhof, Phys. Rev. Lett. **77**, 3865 (1996).
[68] J. VandeVondele and J. Hutter, J. Chem. Phys. **127**, 114105 (2007).
[69] S. Goedecker, M. Teter, and J. Hutter, Phys. Rev. B **54**, 1703 (1996).
[70] M. Krack, Theor. Chem. Acc. **114**, 145 (2005).
[71] W. F. Murphy, J. Chem. Phys. **67**, 5877 (1977).
[72] G. Jancso and W. A. Van Hook, Chem. Rev. **74**, 689 (1974).
[73] L. B. Skinner, C. Huang, D. Schlesinger, L. G. Pettersson, A. Nilsson, and C. J. Benmore, J. Chem. Phys. **138**, 074506 (2013).
[74] M. Neumann, Mol. Phys. **50**, 841 (1983).
[75] K. A. Motakabbir and M. Berkowitz, J. Phys. Chem. **94**, 8359 (1990).
[76] I. G. Tironi and W. F. Van Gunsteren, Mol. Phys. **83**, 381 (1994).
[77] H. Yu, T. Hansson, and W. F. Van Gunsteren, J. Chem. Phys. **118**, 221 (2003).
[78] B. Dünweg and K. Kremer, J. Chem. Phys. **99**, 6983 (1993).
[79] I.-C. Yeh and G. Hummer, J. Phys. Chem. B **108**, 15873 (2004).
[80] G. S. Kell, J. Chem. Eng. Data **20**, 97 (1975).
[81] U. Kaatze, J. Chem. Eng. Data **34**, 371 (1989).

[82]K. Krynicki, C. D. Green, and D. W. Sawyer, Faraday Discuss. Chem. Soc. **66**, 199 (1978).
[83]K. R. Harris and L. A. Woolf, J. Chem. Eng. Data **49**, 1064 (2004).
[84]G. S. Kell, J. Chem. Eng. Data **12**, 66 (1967).
[85]S. Iuchi, A. Morita, and S. Kato, J. Phys. Chem. B **106**, 3466 (2002).
[86]R. Ramírez, T. López-Ciudad, P. Kumar P, and D. Marx, J. Chem. Phys. **121**, 3973 (2004).
[87]Z.-H. Xu and M. Meuwly, J. Phys. Chem. A **121**, 5389 (2017).
[88]K. Mackeprang, Z.-H. Xu, Z. Maroun, M. Meuwly, and H. G. Kjaergaard, Phys. Chem. Chem. Phys. **18**, 24654 (2016).
[89]C. Vega and J. L. F. Abascal, Phys. Chem. Chem. Phys. **13**, 19663 (2011).